Analytical Derivation and Design of 20-MHz DC–DC Soft-Switching Resonant Converter

Yueshi Guan, *Member, IEEE*, Chang Liu, *Student Member, IEEE*, Yijie Wang, *Senior Member, IEEE*, Wei Wang, and Dianguo Xu, *Fellow, IEEE*

***Abstract*—In this article, a novel 20-MHz high-frequency high-performance dc–dc resonant converter is analyzed, which owns the characteristics of soft-switching, low voltage stress, and small volume. The numerical analysis is conducted in time domain and the resonant parameters can be accurately calculated based on the corresponding expressions. A full resonant rectifier stage is adopted without using choke inductors, and the value and volume of inductors can be greatly reduced. A 12-V input, 5 V/5 W output prototype is proposed in the laboratory and the experimental results verify the feasibility of the proposed converter and numerical design methodology.**

***Index Terms*—DC–DC, high-frequency converter, small volume, soft-switching characteristics.**

I. Introduction

With the fast development of power electronic technology, great demands of high efficiency, small volume, and prediction ability have been put forward for power converters [1]–[6]. High operating frequency can reduce the necessary stored energy of passive components within every period, leading to small value and volume of inductor, transformer, and electrolytic capacitor. Thus, improving the operating frequency is the most effective way to reduce power system volume. Also, with the value reduction of passive components, the parasitic components are in the similar level of required resonant components. Therefore, the parasitic capacitance of semiconductor devices (switch and diode) can be utilized in high operating situations [7]–[11].

However, higher operating frequency causes larger switching loss [12]–[15]. The switches and diodes are expected to operate in soft-switching mode. Hence, a lot of attention has been paid to design a high-frequency converter with well soft-switching characteristics. For tens of MHz dc–dc converters, the typical structure consists of inverter stage, matching network stage, and rectifier stage. Under tens of MHz frequency condition, the ground-reference switch structure is widely adopted, which can simplify the driving circuit compared with float switch and half-bridge structure.

Class E circuit is a typical resonant inverter with well-behaved soft-switching characteristics. However, the voltage stress of Class E circuit is quite high, which is around four times the input voltage [16], [17]. To address this issue, Class Φ_2 circuit with a parallel branch is proposed to reduce voltage stress [18]. In Class Φ_2 circuit, a parallel branch is adopted to adjust the amplitude of high-order harmonics in order to reshape the voltage across the switch. In the rectifier stage, according to duality principle, similar topologies can be adopted to regulate ac components to constant dc value, such as current-driven Class E rectifier stage [19]. In the rectifier, diode can be used to replace the switch. Also, the synchronous rectifier based on switch shows good performance on low conduction loss, especially for large output current situation.

However, for the Class Φ_2 inverter, because of the complex resonance during the operating period, expressions of current and voltage in time domain have not been established. The characteristics in frequency domain, such as locations of poles, are adopted to design system parameters [20]–[26]. The approximation in this method leads to the shift of the working point, resulting in the switching loss and the output error. Since the abovementioned problems cannot be solved, the choice of parameters is mainly based on simulation results, which consumes a lot of time. Thus, the accurate parameter expression calculation method should be investigated. In addition, the traditionally used current-driven Class E rectifier uses a choke inductor to provide a constant inductor current, but the inductance is usually at quite a high level, which increases the size of the system [27]. Therefore, it is necessary to redesign the working state of the rectifier and reduce the inductance by resonating with a capacitor.

Matching network stage is a bridge between the inverter stage and rectifier stage, which can adjust the equivalent impedance of rectifier stage to meet the requirement of inverter stage. Matching network can be divided into isolated one and nonisolated one [28], [29]. For isolated matching network, transformer, especially aircore transformer, is adopted to achieve impedance adjustment. For nonisolated situation, L-type matching network is the simplest one and widely adopted in high-frequency dc–dc converter, which only consists of one inductor and one capacitor. It can achieve resistive to resistive transformation at designed operating frequency. However, this matching network is

Manuscript received June 17, 2019; revised September 24, 2019 and December 2, 2019; accepted December 24, 2019. Date of publication January 15, 2020; date of current version October 19, 2020. This work was supported in part by the National Natural Science Foundation of China under Grant 51777038 and in part by the Youth Talent Project of Harbin Institute of Technology (HIT). *(Corresponding author: Yijie Wang.)*

The authors are with the School of Electrical Engineering and Automation, HIT, Harbin 150001, China (e-mail: hitguanyueshi@163.com; 18800428682@163.com; wangyijie@hit.edu.cn; wangwei602@hit.edu.cn; xudiang@hit. edu.cn).

Color versions of one or more of the figures in this article are available online at http://ieeexplore.ieee.org.

Digital Object Identifier 10.1109/TIE.2020.2965508

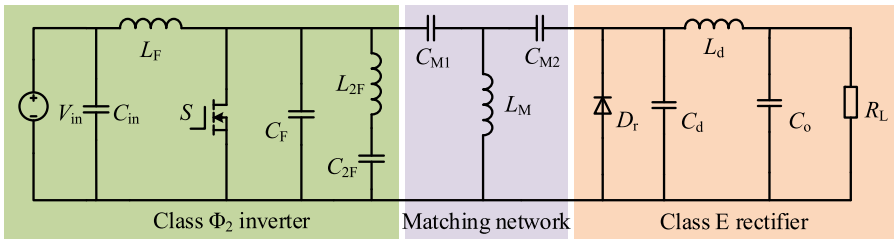

Fig. 1. Proposed high-frequency converter based on Class Φ_2 inverter, T-type matching network, and Class E rectifier.

difficult to achieve an inductive to resistive transformation when the rectifier is inductive. Thus, a network with more flexible transformation ability should be proposed.

In this article, the detailed analytic derivation of Class Φ_2 inverter is demonstrated, which provides an accurate model and parameter design methodology in time domain. A full resonant rectifier stage is adopted without the use of choke inductors.

Also, the T-type matching network with inductive to resistive transformation ability is designed. The proposed numerical design method can help guarantee soft-switching characteristics of the high-frequency converter. The detailed analysis of Class Φ_2 inverter is depicted in Section II. Section III analyzes the rectifier and matching network. The driving, control method, and experimental results of 20-MHz prototype are given in Section IV. Section V concludes this article.

II. Analysis and Analytical Derivation of Class Φ_2 Inverter

The circuit diagram of the proposed converter is shown in Fig. 1. It consists of a Class Φ_2 inverter, a T-type matching network, and a Class E resonant rectifier. The Class Φ_2 inverter converts the dc component to ac component. Compared with the Class E inverter, a parallel branch composed of L_{2F} and C_{2F} is added to resonate with L_F, C_F, and the poststage equivalent impedance, thus, the third harmonic can be enhanced and the second harmonic is suppressed, which effectively reduces the voltage stress of the switch. The role of the T-type matching network is to adjust the equivalent input impedance of the rectifier, in order to meet the output impedance requirement of inverter stage. The T matching network can adjust the phase and amplitude simultaneously, which helps to ensure zero voltage switching (ZVS) characteristics of the switch. The rectifier regulates the ac component to dc output component, a Class E resonant rectifier is adopted in this article to guarantee the zero current switching (ZCS) characteristics of the diode. In previous researches, the design of high-frequency converters are mostly based on parametric scanning, which is very time-consuming and the parameters may not be optimal. Thus, numerical analysis is adopted in this article to realize the precise parameter design of the system.

Fig. 2 shows the circuit structure of Class Φ_2 inverter, the voltage stress of the switch can be effectively reduced by harmonic adjustment. The traditional method to design this inverter is usually based on frequency-domain analysis and circuit simulation results, which causes huge time wastage and parameter errors. Thus, to improve the design speed and accuracy of this

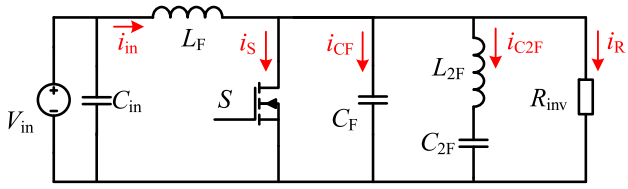

Fig. 2. Diagram of Class Φ_2 inverter.

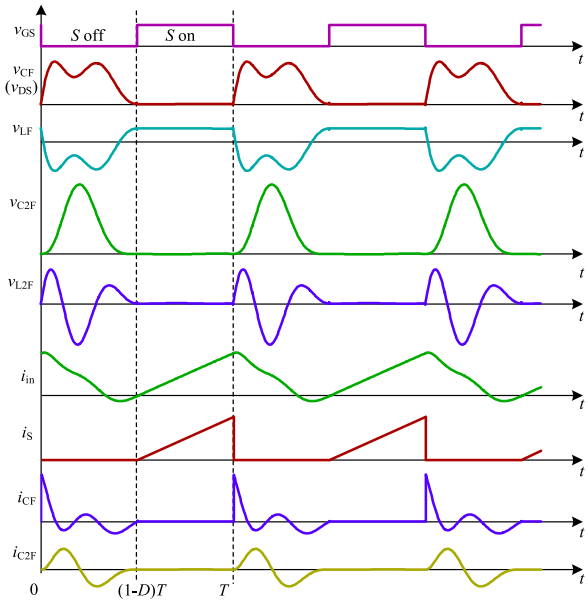

Fig. 3. Waveforms of the inverter.

stage, the numerical method in time domain will be adopted to realize the theoretical analysis of the inverter.

Fig. 3 shows the current and voltage waveforms of the inverter. When $(1-D)T \le t \le T$, the switch is in ON state, $v_{LF} = V_{\text{in}}$, $v_{L2F} + v_{C2F} = 0$, that is to say, the inductor L_F is charged by the input voltage source during this period, thus, its voltage increases linearly. Meanwhile, L_{2F} and C_{2F} resonate in series; the differential equation for v_{C2F} can be derived as

$$\frac{d^2 v_{C2F}}{dt^2} + \frac{1}{L_{2F}C_{2F}} v_{C2F} = 0 \tag{1}$$

and its general solution can be obtained

$$v_{C2F} = H_1 \cos\frac{t}{\sqrt{L_{2F}C_{2F}}} + H_2 \sin\frac{t}{\sqrt{L_{2F}C_{2F}}}. \tag{2}$$

Considering the existence of parasitic resistance of the resonant components, the resonant current in L_{2F} and C_{2F} series branch will generate unexpected power losses, reducing the system efficiency. In fact, compared with Class E inverter, the L_{2F} and C_{2F} series branch is introduced in Class Φ_2 inverter, which resonates with other components, thereby introducing corresponding higher harmonics and reducing the voltage stress of the switch. In this article, for the purpose of balancing the voltage stress of the switch and the efficiency of the system, the series branch is designed to participate in resonance only during the switch-OFF period, and the series resonance between L_{2F} and C_{2F} does not occur when the switch is ON. With this design method, the voltage stress during the switch-OFF period will still be effectively reduced, and the additional losses will not be introduced. To ensure that the series resonance does not occur, the following conditions should be satisfied:

$$\begin{cases} v_{C2F}(t)\big|_{t=(1-D)T} = 0 \\ C_{2F}\frac{dv_{C2F}(t)}{dt}\big|_{t=(1-D)T} = 0 \end{cases}. \tag{3}$$

Combining (2) and (3), it can be obtained that $H_1 = H_2 = 0$, which means that v_{C2F} is always zero during the switch-ON period, and there is no reactive current in the branch, avoiding additional losses.

When $0 \le t \le (1-D)T$, the switch is in OFF state, according to KCL, the following equation can be obtained:

$$i_{\text{in}} = i_{CF} + i_{C2F} + i_R. \tag{4}$$

The inductor L_F of the Class Φ_2 inverter operates in resonant state, so the current i_{in} will flow in positive and negative directions as Fig. 3 shows. A paralleled capacitor in the input side of the Class Φ_2 inverter is usually used which buffers the energy and stabilizes the input voltage.

Since the derivatives of these current equations satisfy

$$\begin{cases} \frac{di_{\text{in}}}{dt} = \frac{V_{\text{in}} - v_{CF}}{L_F} \\ \frac{di_{CF}}{dt} = \frac{d}{dt}\left(C_F\frac{dv_{CF}}{dt}\right) = C_F\frac{d^2v_{CF}}{dt^2} \\ \frac{di_{C2F}}{dt} = \frac{d}{dt}\left(C_{2F}\frac{dv_{C2F}}{dt}\right) = C_{2F}\frac{d^2v_{C2F}}{dt^2} \\ \frac{di_R}{dt} = \frac{d}{dt}\left(\frac{v_{CF}}{R_{\text{inv}}}\right) = \frac{1}{R_{\text{inv}}}\frac{dv_{CF}}{dt} \end{cases} \tag{5}$$

it can be derived that

$$\frac{V_{\text{in}} - v_{CF}}{L_F} = C_F\frac{d^2v_{CF}}{dt^2} + C_{2F}\frac{d^2v_{C2F}}{dt^2} + \frac{1}{R_{\text{inv}}}\frac{dv_{CF}}{dt}. \tag{6}$$

Besides, the voltage of C_F can be expressed as

$$\begin{aligned} v_{CF} = v_{L2F} + v_{C2F} &= L_{2F}\frac{di_{C2F}}{dt} + v_{C2F} \\ &= L_{2F}C_{2F}\frac{d^2v_{C2F}}{dt^2} + v_{C2F}. \end{aligned} \tag{7}$$

Combining (6) and (7), the following differential equation can be obtained:

$$\begin{cases} C_{2F}\frac{d^2v_{C2F}}{dt^2} + C_F\frac{d^2v_{CF}}{dt^2} + \frac{1}{R}\frac{dv_{CF}}{dt} + \frac{v_{CF}}{L_F} = \frac{V_{\text{in}}}{L_F} \\ L_{2F}C_{2F}\frac{d^2v_{C2F}}{dt^2} + v_{C2F} - v_{CF} = 0 \end{cases} \tag{8}$$

where v_F and v_{2F} are the instantaneous voltages of C_F and C_{2F}, respectively. A fourth-order differential equation can be obtained, according to (8), as follows:

$$\begin{aligned} &L_FC_FL_{2F}C_{2F}\frac{d^4v_{C2F}}{dt^4} + \frac{L_FC_FC_{2F}}{R}\frac{d^3v_{C2F}}{dt^3} \\ &+ (L_FC_{2F} + L_FC_F + L_{2F}C_{2F})\frac{d^2v_{C2F}}{dt^2} \\ &+ \frac{L_F}{R}\frac{dv_{C2F}}{dt} + v_{C2F} = V_{\text{in}}. \end{aligned} \tag{9}$$

By introducing a series of intermediate variables (α_1, β_1, α_2, β_2 and coefficients A_1, A_2, A_3, A_4, A_5), it can help to express and calculate the circuit resonant parameters. Here, the roots of the characteristic equation of (9) can be expressed by (10), and the solution of (9) can be expressed by (11) in the following:

$$r_{1,2} = \frac{\alpha_1 \pm j\beta_1}{(1-D)T}, \quad r_{3,4} = \frac{\alpha_2 \pm j\beta_2}{(1-D)T} \tag{10}$$

$$\begin{cases} v_{C2F}(t) = e^{\frac{\alpha_1}{(1-D)T}t}\left(A_1\cos\frac{\beta_1}{(1-D)T}t + A_2\sin\frac{\beta_1}{(1-D)T}t\right) \\ \qquad + e^{\frac{\alpha_2}{(1-D)T}t}\left(A_3\cos\frac{\beta_2}{(1-D)T}t + A_4\sin\frac{\beta_2}{(1-D)T}t\right) \\ \qquad + A_5 \ 0 \le t \le (1-D)T \\ v_{CF}(t) = \frac{(\alpha_1+\alpha_2)(1-D)^2T^2}{\alpha_1\left(\alpha_2^2+\beta_2^2\right)+\alpha_2\left(\alpha_1^2+\beta_1^2\right)} \cdot \frac{d^2v_{C2F}}{dt^2} + v_{C2F} \ 0 \le t \\ \qquad \le (1-D)T \end{cases} \tag{11}$$

In the next three paragraphs, the conditions of the system are found and used to solve the intermediate parameters A_1–A_5 and α_1, β_1, α_2, β_2.

First, based on previous analysis, since L_{2F} and C_{2F} do not resonate with each other during the switch-ON period, v_{C2F} and i_{C2F} are always zero. Thus, it can be known that $v_{C2F}(0) = v_{C2F}(T) = 0$ and $i_{C2F}(0) = i_{C2F}(T) = 0$. Taking $i_{C2F} = C_{2F}(dv_{C2F}/dt)$ into consideration, the following two conditions can be obtained:

$$\begin{cases} v_{C2F}(0) = 0 \\ \frac{dv_{C2F}}{dt}\big|_{t=0} = 0 \end{cases}. \tag{12}$$

Meanwhile, for the switch, its voltage v_{ds} (v_{CF}) starts to change from zero at the moment when S is turned OFF. And v_{ds} resonates to zero and satisfies $dv_{ds}/dt = 0$ when S is just turned ON, so that the switch can achieve ZVS and zero derivative voltage switching (ZdVS) characteristics. That is

$$\begin{cases} v_{CF}(0) = 0 \\ v_{CF}(t)\big|_{t=(1-D)T} = 0 \\ \frac{dv_{CF}}{dt}\big|_{t=(1-D)T} = 0 \end{cases}. \tag{13}$$

In addition, the input current of the system i_{in} can be expressed as follows during the ON and OFF period:

$$\begin{cases} i_{\text{in}}(0) = i_{CF}(0) + i_{C2F}(0) + i_R(0) = C_F\frac{dv_{CF}}{dt}\big|_{t=0} \\ i_{\text{in}}((1-D)T) = [i_{CF}(t) + i_{C2F}(t) + i_R(t)]\big|_{t=(1-D)T} = 0 \end{cases} \tag{14}$$

$$\begin{cases} i_{\text{in}}(0) = i_{\text{in}}(T) = i_{\text{in}}((1-D)T) + \frac{1}{L_F}\int_{(1-D)T}^{T} v_{LF}dt \\ \quad = \frac{DTV_{\text{in}}}{L_F} \\ i_{\text{in}}((1-D)T) = i_{\text{in}}(0) + \frac{1}{L_F}\int_{0}^{(1-D)T} v_{LF}dt \\ \quad = \frac{TV_{\text{in}}}{L_F} - \frac{1}{L_F}\int_{0}^{(1-D)T} v_{CF}dt \end{cases}. \tag{15}$$

Solving (14) and (15), the following two conditions of the system can be obtained:

$$\begin{cases} \frac{dv_{CF}}{dt}|_{t=0} = \frac{DTV_{\text{in}}}{L_F C_F} \\ \int_0^{(1-D)T} v_{CF}dt = TV_{\text{in}} \end{cases}. \tag{16}$$

Substituting the nine condition equations included by (3), (12), (13), and (16) into (9), the following formula can be obtained:

$$M\begin{bmatrix} A_1 & A_2 & A_3 & A_4 \end{bmatrix}^T = \frac{\left(\alpha_1^2+\beta_1^2\right)\left(\alpha_2^2+\beta_2^2\right)V_{in}}{1-D} \times \begin{bmatrix} 0 & 0 & 0 & 0 & 0 & 0 & D & 1 \end{bmatrix}^T \tag{17}$$

where $M = [M_1 \mid M_2]$, M_1 and M_2 satisfy (18) shown at the bottom of this page. It is also worth noting that there are nine conditions for (9), so nine equations should be obtained; but as seen from (17), there are only eight equations. This is because $A_5 = -A_1 - A_3$ according to $v_{C2F}(0) = 0$, A_5 is replaced by $-A_1 - A_3$ to reduce the order of the equations and simplify the form of (17). In fact, (18) is a set of equations about α_1, β_1, α_2, β_2, and A_1–A_5 synthesized by various conditions. The appendix shows how to split and solve these variables. By solving this system of equations numerically in MATLAB, it can be concluded that α_1, β_1, α_2, and β_2 are only determined by the duty cycle D of the switch and A_1–A_5 are only determined by the duty cycle D and the input voltage V_{in}. When $D = 0.5$, the solution of (17) is shown in Table I.

TABLE I
NUMERICAL SOLUTION OF (16) WHEN $D = 0.5$

label	value	label	value
A_1	-1.746V_{in}	α_1	-1.5321
A_2	5.910V_{in}	α_2	-2.3940
A_3	0.746V_{in}	β_1	4.5971
A_4	-2.581V_{in}	β_2	10.8680
A_5	V_{in}		

According to the duty cycle D, cycle T, and load R of the inverter, by substituting intermediate variables $\alpha_1, \beta_1, \alpha_2, \beta_2$ into (19) shown at the bottom of this page, the resonant parameters of the inverter can be solved.

$$\begin{cases} M_1 = \begin{bmatrix} e^{\alpha_1}\cos\beta_1 - 1 & e^{\alpha_1}\sin\beta_1 \\ \alpha_1 & \beta_1 \\ e^{\alpha_1}\left(\alpha_1\cos\beta_1 - \beta_1\sin\beta_1\right) & e^{\alpha_1}\left(\alpha_1\sin\beta_1 + \alpha_1\cos\beta_1\right) \\ \alpha_1^2 - \beta_1^2 & 2\alpha_1\beta_1 \\ e^{\alpha_1}\left[\left(\alpha_1^2-\beta_1^2\right)\cos\beta_1 - 2\alpha_1\beta_1\sin\beta_1\right] & e^{\alpha_1}\left[2\alpha_1\beta_1\cos\beta_1 + \left(\alpha_1^2-\beta_1^2\right)\sin\beta_1\right] \\ e^{\alpha_1}\left[\alpha_1\left(\alpha_1^2-3\beta_1^2\right)\cos\beta_1 - \beta_1\left(3\alpha_1^2-\beta_1^2\right)\sin\beta_1\right] & e^{\alpha_1}\left[\beta_1\left(3\alpha_1^2-\beta_1^2\right)\cos\beta_1 + \alpha_1\left(\alpha_1^2-3\beta_1^2\right)\sin\beta_1\right] \\ \alpha_1\left(\alpha_1^2-3\beta_1^2\right) & \beta_1\left(3\alpha_1^2-\beta_1^2\right) \\ \left(\alpha_2^2+\beta_2^2\right)\left[e^{\alpha_1}\left(\alpha_1\cos\beta_1 + \beta_1\sin\beta_1\right) - \alpha_1 - \left(\alpha_1^2+\beta_1^2\right)\right] & \left(\alpha_2^2+\beta_2^2\right)\left[e^{\alpha_1}\left(\alpha_1\sin\beta_1 - \beta_1\cos\beta_1\right) + \beta_1\right] \end{bmatrix} \\ M_2 = \begin{bmatrix} e^{\alpha_2}\cos\beta_2 - 1 & e^{\alpha_2}\sin\beta_2 \\ \alpha_2 & \beta_2 \\ e^{\alpha_2}\left(\alpha_2\cos\beta_2 - \beta_2\sin\beta_2\right) & e^{\alpha_2}\left(\alpha_2\sin\beta_2 + \beta_2\cos\beta_2\right) \\ \alpha_2^2 - \beta_2^2 & 2\alpha_2\beta_2 \\ e^{\alpha_2}\left[\left(\alpha_2^2-\beta_2^2\right)\cos\beta_2 - 2\alpha_2\beta_2\sin\beta_2\right] & e^{\alpha_2}\left[2\alpha_2\beta_2\cos\beta_2 + \left(\alpha_2^2-\beta_2^2\right)\sin\beta_2\right] \\ e^{\alpha_2}\left[\alpha_2\left(\alpha_2^2-3\beta_2^2\right)\cos\beta_2 - \beta_2\left(3\alpha_2^2-\beta_2^2\right)\sin\beta_2\right] & e^{\alpha_2}\left[\beta_2\left(3\alpha_2^2-\beta_2^2\right)\cos\beta_2 + \alpha_2\left(\alpha_2^2-3\beta_2^2\right)\sin\beta_2\right] \\ \alpha_2\left(\alpha_2^2-3\beta_2^2\right) & \beta_2\left(3\alpha_2^2-\beta_2^2\right) \\ \left(\alpha_1^2+\beta_1^2\right)\left[e^{\alpha_2}\left(\alpha_2\cos\beta_2 + \beta_2\sin\beta_2\right) - \alpha_2 - \left(\alpha_2^2+\beta_2^2\right)\right] & \left(\alpha_1^2+\beta_1^2\right)\left[e^{\alpha_2}\left(\alpha_2\sin\beta_2 - \beta_2\cos\beta_2\right) + \beta_2\right] \end{bmatrix} \end{cases} \tag{18}$$

$$\begin{cases} L_F = -\dfrac{2\alpha_1\left(\alpha_2^2+\beta_2^2\right) + 2\alpha_2\left(\alpha_1^2+\beta_1^2\right)}{\left(\alpha_1^2+\beta_1^2\right)\left(\alpha_2^2+\beta_2^2\right)}(1-D)TR \quad C_F = -\dfrac{(1-D)T}{2\left(\alpha_1+\alpha_2\right)R} \\ L_{2F} = -\dfrac{2(\alpha_1+\alpha_2)^2\left[\alpha_1\left(\alpha_2^2+\beta_2^2\right) + \alpha_2\left(\alpha_1^2+\beta_1^2\right)\right]}{\alpha_1\alpha_2\left\{\left(\alpha_1^2+\beta_1^2-\alpha_2^2-\beta_2^2\right)^2 + 4\left(\alpha_1+\alpha_2\right)\left[\alpha_1\left(\alpha_2^2+\beta_2^2\right) + \alpha_2\left(\alpha_1^2+\beta_1^2\right)\right]\right\}}(1-D)TR \\ C_{2F} = -\dfrac{\alpha_1\alpha_2\left\{\left(\alpha_1^2+\beta_1^2-\alpha_2^2-\beta_2^2\right)^2 + 4\left(\alpha_1+\alpha_2\right)\left[\alpha_1\left(\alpha_2^2+\beta_2^2\right) + \alpha_2\left(\alpha_1^2+\beta_1^2\right)\right]\right\}}{2\left(\alpha_1+\alpha_2\right)\left[\alpha_1\left(\alpha_2^2+\beta_2^2\right) + \alpha_2\left(\alpha_1^2+\beta_1^2\right)\right]^2 R}(1-D)T \end{cases} \tag{19}$$

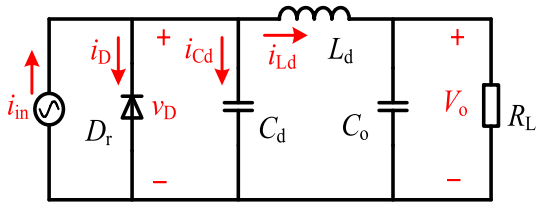

Fig. 4. Current-driven Class E resonant rectifier.

III. Analysis of Class E Rectifier and T Type Matching Network

Fig. 4 shows the circuit of the Class E resonant rectifier adopted in this article, which is driven by $i_{\text{in}}(t) = I_{\text{in}}\sin(\omega t + \varphi)$, where I_{in}, ω, and φ represent the current magnitude, angular frequency, and initial phase angle, respectively. Here, D_d is the duty cycle of the diode D_r.

In order to simplify the analysis of this stage, we assume that:

1) the output capacitor C_o is large enough so the output voltage V_o has no ripple;
2) all devices are ideal, that is, the forward voltage drop of the diode and equivalent series resistances (ESRs) of the passive components are ignored.

The voltage and current waveforms of the rectifier are shown in Fig. 5; it can be seen that the current of the diode i_D can resonate to zero, achieving ZCS characteristic. When $0 \le t \le (1 - D_d)T$, the diode is in OFF state, according to KCL and KVL, the following differential equation can be obtained:

$$\frac{d^2 v_D}{dt^2} + \frac{1}{L_d C_d} \cdot v_D - \frac{\omega L_d I_{\text{in}} \cos(\omega t + \varphi) - V_o}{L_d C_d} = 0. \quad (20)$$

Then, the voltage of the diode v_D is solved, Equation (21) shown at the bottom of this page,

where $\omega_d = 1/\sqrt{L_d C_d}$. Meanwhile, the current of the inductor L_d is derived as Equation (22) shown at the bottom of this page.

Because of resonance, the current i_{Ld} is bidirectional. During the analysis of the rectification part, the input part of the rectifier is represented by a current source. In the complete proposed topology, the rectifier part follows the inverter and matching network. Thus, the energy can be drawn from the inverter and matching network and can also be returned to the inverter and matching network.

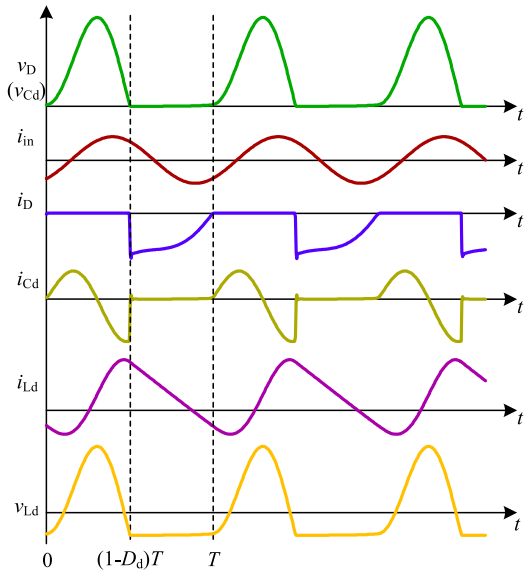

Fig. 5. Waveforms of rectifier.

According to the volt–second balance of the inductor L_d and the amp–second balance of the capacitor C_d, (23) can be obtained as follows:

$$\begin{cases} \frac{1}{T}\int_0^T v_D(t)\,dt = V_o \\ \frac{1}{T}\int_0^T i_{Ld}(t)\,dt = \frac{P_o}{V_o} \end{cases}. \quad (23)$$

Besides, the diode voltage is zero when $t = (1 - D_d)T$, that is, $v_D((1 - D_d)T) = 0$. Substituting these three constraints into (21) and (22), (24) shown at the bottom of next page, can be easily derived, where $T_{\text{on}} = D_d T$ and $T_{\text{off}} = (1 - D_d)T$, D_d is the conduction ratio of the diode. It can be seen that the variables of (24) are C_d, ω_d, and φ; their numerical solution can be calculated by MATLAB when ω, P_o, V_o, I_{in}, and D_d are known.

Actually, the change of I_{in} and D_d can significantly affect the voltage stress of the diode and the phase angle of the equivalent input impedance of the rectifier. Fig. 6 shows the curve of the nominal diode voltage stress $V_{D\max}/V_o$ and the

$$v_D(t) = \begin{cases} \frac{I_{\text{in}}}{C_d} \cdot \frac{(\omega\sin\omega t - \omega_d \sin\omega_d t)\sin\varphi + \omega(\cos\omega_d t - \cos\omega t)\cos\varphi}{\omega^2 - \omega_d^2} \\ -\frac{I_{\text{in}}}{C_d} \cdot \frac{\sin\omega_d t \sin\varphi}{\omega_d} + V_o(1 - \cos\omega_d t), \quad 0 \le t \le (1 - D_d)T \\ 0, \qquad\qquad (1 - D_d)T \le t \le T \end{cases} \quad (21)$$

$$i_{Ld}(t) = \begin{cases} \frac{(\omega^2\cos\omega_d t - \omega_d^2\cos\omega t)\sin\varphi + \omega\omega_d(\sin\omega_d t - \sin\omega t)\cos\varphi}{\omega^2 - \omega_d^2} I_{\text{in}} \\ -V_o\omega_d C_d \sin\omega_d t, \qquad 0 \le t \le (1 - D_d)T \\ i_{Ld}((1 - D_d)T) - V_o\omega_d^2 C_d[t - (1 - D_d)T], \quad (1 - D_d)T \le t \le T \end{cases} \quad (22)$$

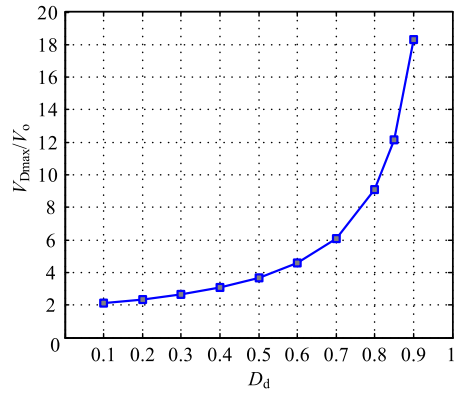

Fig. 6. Relationship between $V_{D\max}$, V_o, and D_d.

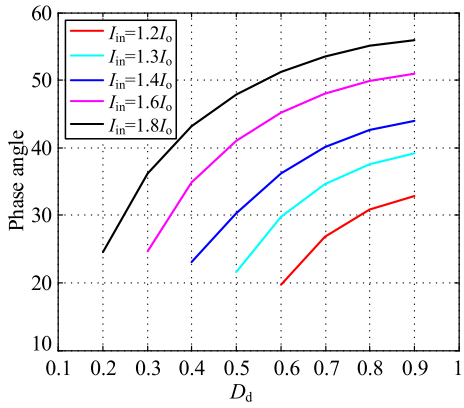

Fig. 7. Relationship between $\varphi_{\rm rec}$, $I_{\rm in}$, and D_d.

diode ratio D_d, it can be seen that $V_{D\max}/V_o$ increases sharply as D_d increases, thus resulting in an increasing voltage stress. During the circuit design process, the input and output voltages are taken as determined parameters. For the diode, the forward conduction voltage usually forms a proportional relationship with the rated voltage. Hence, higher voltage stress leads to higher diode conduction loss. In addition, for the purpose of analyzing the input impedance characteristics of the rectifier, Fourier analysis is performed on (21) to obtain

$$v_D(t) = V_o + \sum_{n=1}^{\infty} V_{\mathbf{D}n}\sin(n\omega t + \varphi_n). \tag{25}$$

Here, the amplitude V_{Dn} and the phase angle φ_n of the nth harmonic satisfy

$$\begin{cases} V_{Dn} = \frac{2}{T} \\ \quad \times\sqrt{\left(\int_0^T v_D(t)\cos(n\omega t)\,dt\right)^2 + \left(\int_0^T v_D(t)\sin(n\omega t)\,dt\right)^2} \\ \varphi_n = \arctan\left(\int_0^T v_D(t)\cos(n\omega t)\,dt \right. \\ \quad \left. \Big/ \int_0^T v_D(t)\sin(n\omega t)\,dt\right) \end{cases}. \tag{26}$$

Then, the input impedance of the rectifier can be written as $Z_{\rm rec} = (V_{D1}/I_{\rm in})\angle(\varphi_n - \varphi)$.

Fig. 7 shows the relationship between the phase angle $\varphi_{\rm rec}(=\varphi_n - \varphi)$, $I_{\rm in}$, and D_d when $P_o = 5$ W and $V_o = 5$ V. It can be seen that $\varphi_{\rm rec}$ increases as $I_{\rm in}$ or D_d increases. According to Figs. 6 and 7, the selected $I_{\rm in}$ and D_d should promise moderate $V_{D\max}$ and small $\varphi_{\rm rec}$, so that the rectifier can operate efficiently and reliably. Then, the resonant parameters can be calculated by MATLAB easily.

Fig. 8 shows the parameter curves of L_d and C_d with different $I_{\rm in}$ and D_d under the condition of $P_o = 5$ W, $V_o = 5$ V, and $f = 20$ MHz, which provides a reference for the selection of resonant parameters. Here, the resonant inductor increases as duty D_d increases, and the resonant capacitor decreases as duty D_d increases.

In HF and VHF systems, the L matching network, as shown in Fig. 9, is often used due to its small number of components, simple structure and high efficiency. In the original design, this article intended to adopt this network to transfer the equivalent input impedance of the rectifier $Z_{\rm rec}$ to a pure resistor $R_{\rm inv}$ at the switching frequency, so that the system can meet its power requirement and the switch can operate in soft-switching condition.

The rectifier is inductive at the switching frequency, and its input impedance can be represented by $Z_{\rm rec} = R_{\rm rec} + jX_{\rm rec}$. The impedance after transforming through the matching network is expected to satisfy $Z_{\rm inv} = R_{\rm inv} = V_{DS\mathbf{1}}^2/(2P_o)$, where V_{DS1} is the amplitude of the fundamental component of v_{DS} (the output voltage of Class Φ_2 inverter). The expression of $Z_{\rm inv}$ can be calculated as

$$Z_{{\rm in}v} = \frac{s^2 L_S C_S Z_{\rm rec} + sL_S + Z_{\rm rec}}{s^2 L_S C_S + sC_S Z_{\rm rec}}. \tag{27}$$

$$\begin{cases} \frac{I_{\rm in}}{C_d}\left[\frac{(\omega\sin\omega T_{\rm off} - \omega_d\sin\omega_d T_{\rm off})\sin\varphi + \omega(\cos\omega_d T_{\rm off} - \cos\omega T_{\rm off})\cos\varphi}{\omega^2 - \omega_d^2} - \frac{\sin\omega_d T_{\rm off}\sin\varphi}{\omega_d}\right] + V_o(1 - \cos\omega_d T_{\rm off}) = 0 \\ \frac{I_{\rm in}}{(\omega^2 - \omega_d^2)\omega_d C_d}\left[\omega_d(\cos\omega_d T_{\rm off} - \cos\omega T_{\rm off})\sin\varphi + (\omega\sin\omega_d T_{\rm off} - \omega_d\sin\omega T_{\rm off})\cos\varphi\right] \\ \quad - \frac{I_{\rm in}(1 - \cos\omega_d T_{\rm off})\sin\varphi}{\omega_d^2 C_d} + \frac{V_o(\omega_d T_{\rm off} - \sin\omega_d T_{\rm off})}{\omega_d} = TV_o \\ \frac{I_{\rm in}}{\omega}\left[\frac{(\omega_d^2\cos\omega T_{\rm off} - \omega^2\cos\omega_d T_{\rm off})\cos\varphi}{\omega^2 - \omega_d^2} + \frac{(\omega^3\sin\omega_d T_{\rm off} - \omega_d^3\sin\omega T_{\rm off})\sin\varphi}{\omega_d(\omega^2 - \omega_d^2)} + \cos\varphi\right] - V_o C_d\left(1 - \cos\omega_d T_{\rm off} + \frac{\omega_d^2 T_{\rm on}^2}{2}\right) \\ + T_{\rm on}\left[\frac{(\omega^2\cos\omega_d T_{\rm off} - \omega_d^2\cos\omega T_{\rm off})\sin\varphi + \omega_d(\omega\sin\omega_d T_{\rm off} - \omega_d\sin\omega T_{\rm off})\cos\varphi}{\omega^2 - \omega_d^2} I_{\rm in} - V_o\omega_d C_d\sin\omega_d T_{\rm off}\right] = \frac{TP_o}{V_o} \end{cases} \tag{24}$$

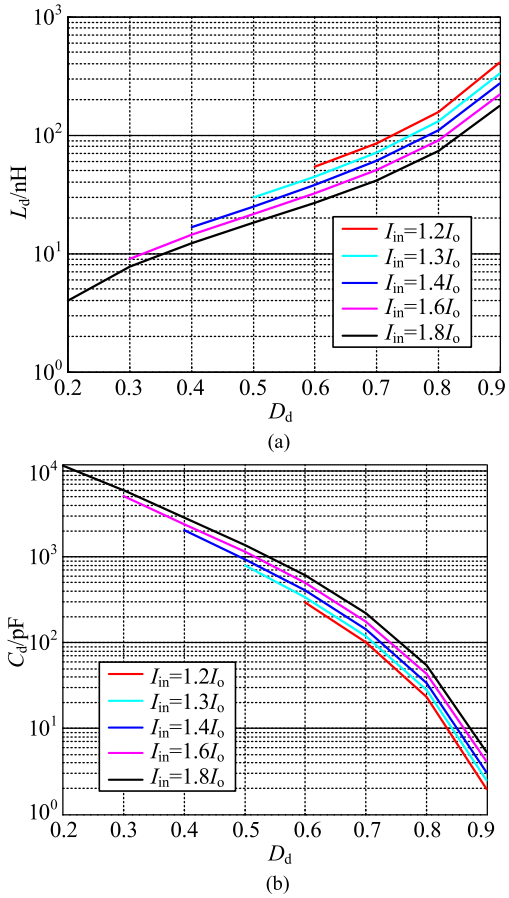

Fig. 8. Parameter curves of L_d and C_d. (a) Relationship between L_d, $I_{\rm in}$, and D_d . (b) Relationship between C_d, $I_{\rm in}$, and D_d.

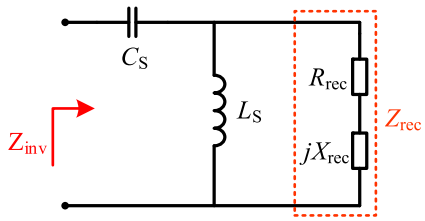

Fig. 9. Circuit of L matching network.

Substituting $Z_{\rm rec} = R_{\rm rec} + jX_{\rm rec}$ and $s = j\omega$ into the above formula, and letting $Z_{\rm inv} = R_{\rm inv}$, the parameters of this stage are calculated as

$$\begin{cases} L_S = \dfrac{X_{\rm rec}R_{\rm inv} + \sqrt{R_{\rm rec}R_{\rm inv}\left(R_{\rm rec}^2 + X_{\rm rec}^2 - R_{\rm rec}R_{\rm inv}\right)}}{\omega\left(R_{\rm rec} - R_{\rm inv}\right)} \\ C_S = \dfrac{1}{\omega}\sqrt{\dfrac{R_{\rm rec}}{R_{\rm inv}\left(R_{\rm rec}^2 + X_{\rm rec}^2 - R_{\rm rec}R_{\rm inv}\right)}} \end{cases}. \tag{28}$$

It can be seen that the following conditions should be satisfied in order to ensure the realization of the inductive to resistive transformation:

$$\begin{cases} R_{\rm rec} - R_{\rm inv} > 0 \\ R_{\rm rec}^2 + X_{\rm rec}^2 - R_{\rm rec}R_{\rm inv} > 0 \end{cases}. \tag{29}$$

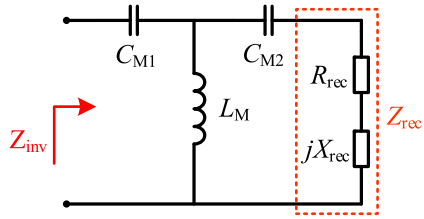

Fig. 10. Circuit of T matching network.

However, the matching network usually adopts to achieve high to low transferring. For prototype specs in Section IV, the impedance can be calculated as $Z_{\rm rec} \approx 5 + j2.5\ \Omega$ and $R_{\rm inv} \approx 23\ \Omega$. Equation (29) cannot be satisfied, thus, the L matching network cannot be used in this article.

To solve this problem, this article considers adding a capacitor to the L matching network to form a T matching network, as shown in Fig. 10. Now, the expression of $Z_{\rm inv}$ can be calculated as

$$Z_{\rm inv} = \frac{s^3L_MC_{M1}C_{M2}Z_{\rm rec} + s^2L_M\left(C_{M1}+C_{M2}\right) + sC_{M2}Z_{\rm rec} + 1}{s^3L_MC_{M1}C_{M2} + s^2C_{M1}C_{M2}Z_{\rm rec} + sC_{M1}}. \tag{30}$$

Using the same method, the parameters of T matching network are calculated as

$$\begin{cases} C_{M1} = C_{M2} \\ \quad = \dfrac{\sqrt{R_{\rm rec}\left[X_{\rm rec}^2 + \left(R_{\rm inv} - R_{\rm rec}\right)^2\right]/R_{\rm inv}} - X_{\rm rec}}{\omega\left(R_{\rm rec}R_{\rm inv} - X_{\rm rec}^2 - R_{\rm rec}^2\right)} \\ L_M = \dfrac{1}{\omega^2C_{M1}} - \dfrac{R_{\rm inv}X_{\rm rec}}{\omega\left(R_{\rm inv} - R_{\rm rec}\right)} \end{cases} \tag{31}$$

and to realize the inductive to resistive transformation, the relationship between $R_{\rm inv}$, $R_{\rm rec}$, and $X_{\rm rec}$ should satisfy

$$\begin{cases} R_{\rm rec} - R_{\rm inv} < 0 \\ R_{\rm rec}^2 + X_{\rm rec}^2 - R_{\rm rec}R_{\rm inv} \neq 0 \end{cases}. \tag{32}$$

It can be easily found that (32) is true with a wide range. For the prototype, when $Z_{\rm rec} \approx 5 + j2.5\ \Omega$ and $R_{\rm inv} \approx 23\ \Omega$, it can be calculated that the T matching network can meet the system requirements.

It can be seen that in the proposed circuit, three inductors are used. One major concern is the variation of the inductance. Taken the most serious 5% variation of inductor in matching network, for example, the transferred impedance amplitude variation is within 8%, and the impedance angle variation is within 3.5°. Under this variation condition, the soft-switching characteristics of the inverter are almost unchanged, which is verified by simulation. Similar conclusions can also be obtained for the other two inductors. Besides, the T-type network can be removed when the rectifier equivalent impedance is the same as the required inverter impedance at certain input/output specs. Thus, passive components can be reduced.

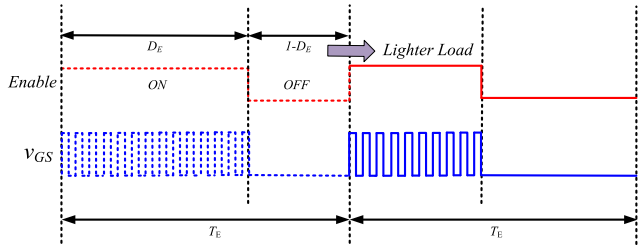

Fig. 11. Diagram of control and driving signal.

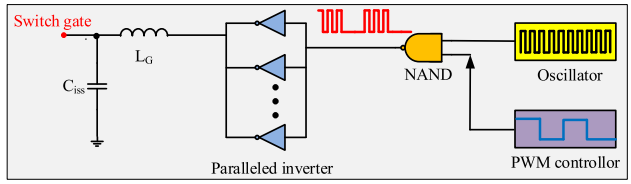

Fig. 12. Driving and control circuit of the converter.

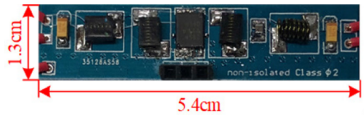

Fig. 13. Prototype of proposed topology.

Based on the abovementioned analysis, the design step of the proposed converter can be summarized as follows. For the converter with specified input/output and frequency requirement, the design procedure is from rectifier stage, to matching network stage, and finally, inverter stage. The diode duty cycle D_d should be determined by considering the voltage stress and circuit loss. Usually, a moderate diode duty cycle is selected around 0.5. Under certain D_d, the equivalent impedance of rectifier stage can be obtained. To match up with the required impedance of inverter stage, the parameters of T-type matching network can be calculated by (31). Finally, the inductance and capacitance parameters of the Class Φ_2 inverter can be calculated by (19) with obtained α_1, β_1, α_2, β_2, and A_1–A_5.

IV. Experimental Results

A 20-MHz, 5 V/5 W with 12 V input voltage prototype is built based on the proposed topology and design method, which helps to verify the feasibility and correctness of the abovementioned design method.

In the prototype, the control circuit regulates the voltage and power through a low-frequency signal as Fig. 11 shows. By adjusting the duty cycle of the pulsewidth modulation (PWM) Enable control signal, the effective operating time can be changed, and the total power of the converter is divided into two parts, as

$$P_O = P_{\text{on}} D_E + P_{\text{off}}(1 - D_E). \tag{33}$$

Since the output power $P_{\text{off}} = 0$ at OFF state and P_{on} remains unchanged at ON state, the total output power P_O is only related to D_E. The output voltage can be controlled by adjusting the duty cycle D_E of the low-frequency signal.

To keep a constant voltage, when the output power decreases from rated power P_{O_R} to light power P_{O_L}, the duty cycle of PWM Enable signal changes from 1 to D_E. Then, the equivalent average power P_{on} during the ON stage can be calculated as

$$P_{\text{on}} = \frac{P_{O\_L}}{D_E} = \frac{P_{O\_R} D_E}{D_E} = P_{O\_R}. \tag{34}$$

From the above equation, it can be seen that in light load operation mode, the equivalent power and voltage seen by the converter does not change under the PWM ON/OFF control (burst fire control) strategy. Thus, with the same output voltage and switching frequency, the switch can maintain soft-switching characteristics under this control method.

Fig. 12 shows the implementation of the driving and control circuit in the prototype. The high-frequency signal and low-frequency Enable signal are combined by a NAND gate, and several paralleled inverters are used to enhance the driving ability. When the operating frequency is at tens of MHz, the resonance of the input parasitic capacitance of the switch can be used in the drive circuit to achieve the purpose of reducing drive loss [30]. In the prototype inductor, L_G resonates with parasitic capacitor C_{iss}, and the driving voltage is in sinusoidal form.

TABLE II
Experimental Parameters of the Prototype

Device label	Value	Type
L_F	82 nH	1812SMS-82N_LC (coilcraft)
L_{2F}, L_M	100 nH	1812SMS-R10_LC (coilcraft)
L_d	56 nH	1812SMS-56N_LC (coilcraft)
C_F	180 pF	ATC700A181(ATC)
C_{2F}	150 pF	ATC700A151(ATC)
C_{M1} ,C_{M2}	680 pF	ATC700A681(ATC)
C_d	300 pF	ATC700A301(ATC)
S	SI7454	Vishay
D_r	STPS2H100A	ST

As shown in Fig. 13, the prototype occupies an area of 1.3 × 5.4 cm^2 and its vertical height is 0.7 cm. The experimental parameters of this system are given in Table II. DPO4014B (Tektronix) is used as the oscilloscope in the experiment, the voltage probe is P6139A (Tektronix), and the voltage source is DP832A (RIGOL).

The waveforms of the prototype under rated working condition are shown in Figs. 14–16. Fig. 14 shows the waveform of the drain-source voltage of the switch v_{ds}. It can be seen that the switch achieves ZVS characteristics very well and the amplitude of v_{ds} is about 32 V, only 2.67 times the input voltage.

Fig. 15 shows the waveform of v_{C2F}, which is generally consistent with the analysis result. However, due to the parasitic inductance of printed circuit board (PCB) layout and passive component (inductance/capacitor) deviation, there are some distortions from the ideal ones.

Fig. 16 shows the waveform of the diode voltage; the voltage stress of the diode is about four times the output voltage and the conduction ratio of the diode is 0.5, which is in good agreement

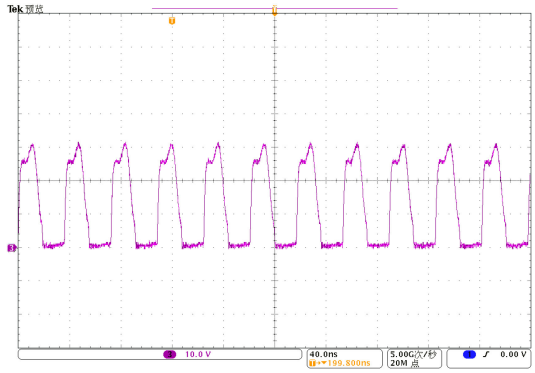

Fig. 14. Experimental waveform of v_{ds}.

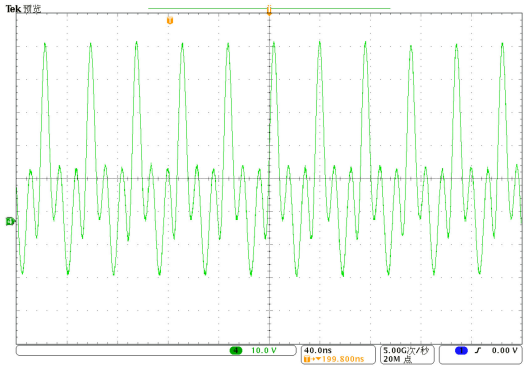

Fig. 15. Experimental waveforms of v_{C2F}.

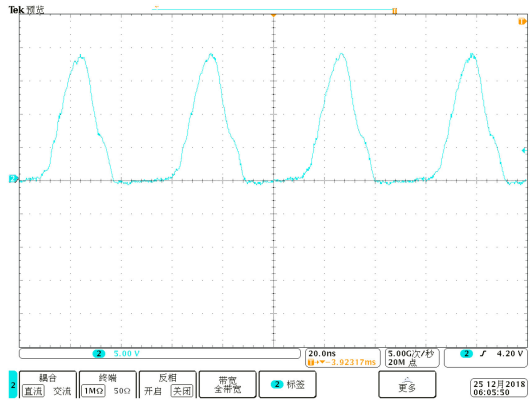

Fig. 16. Experimental waveform of diode.

with the abovementioned theoretical analysis. Fig. 17 shows the waveform of the output voltage.

Constant output voltage under different load conditions can be realized by ON–OFF control, the waveforms of the prototype under ON–OFF control is shown in Figs. 18 and 19. Fig. 18 shows the waveform of v_{ds}, and Fig. 19 shows the waveform of v_{C2F}, illustrating closed-loop performance and soft-switching characteristics of the system.

Fig. 20 shows the efficiency curve of the system under different loads. It can be seen that the efficiency of the system is higher than 80% under different loads, and the highest efficiency is around 82% in the vicinity of rated output power.

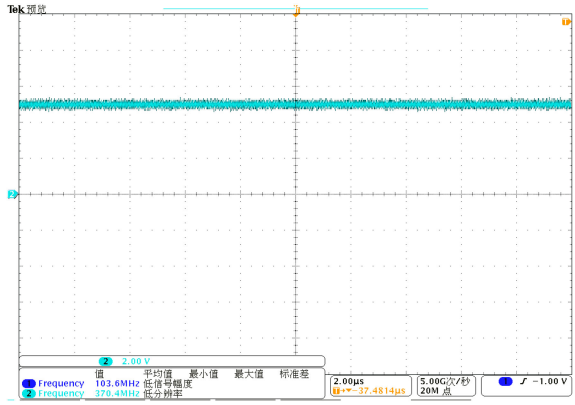

Fig. 17. Waveform of v_O.

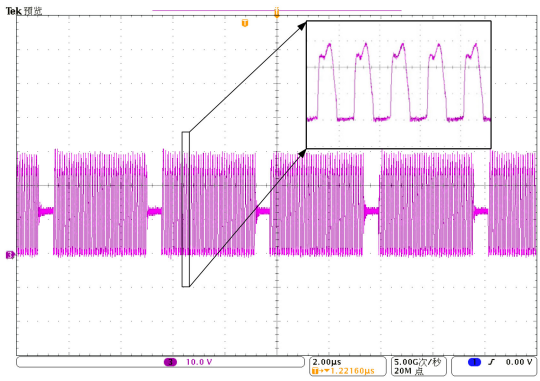

Fig. 18. Waveform of v_{ds} under ON–OFF control.

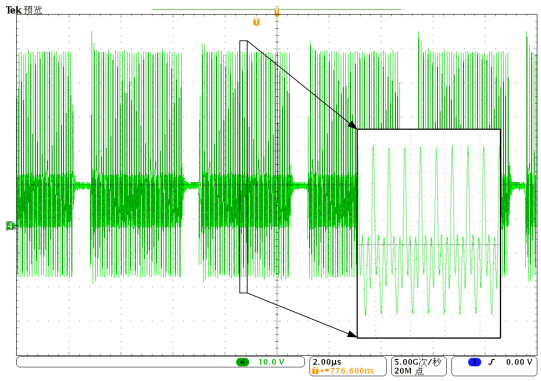

Fig. 19. Waveform of v_{C2F} under ON–OFF control.

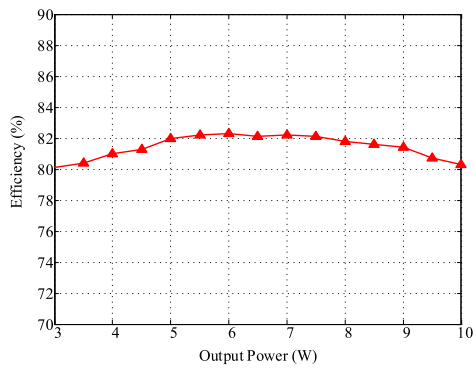

Fig. 20. Efficiency curve of the system under different loads.

The proposed converter has also been tested under higher power, the efficiency begins to reduce when the power is higher. If the current is further increased, the inductor and diode should be reselected to reduce the conduction loss, and the synchronous rectification may be adopted.

V. Conclusion

This article analyzed a 20-MHz high-performance dc–dc resonant converter. In this article, the proposed numerical method was used to analyze the working mode of the circuit in time domain, and the resonant parameters can be accurately calculated. A small resonant inductor was used in the rectifier, rather than a choke inductor, which can reduce the size and help to achieve soft-switching. A 20-MHz, 5 V/5 W with 12 V input voltage prototype was built to verify the feasibility and correctness of the proposed design method. The switch kept low voltage stress characteristics and ZVS characteristics. The system efficiency was about 82% at rated output power.

Appendix

There are eight equations in (17), and the number of unknowns is exactly eight, so the equations can be solved. In order to obtain the specific values of the eight intermediate variables, we first divide α_1, α_2, β_1, β_2, and A_1–A_4 into two groups, that is, when solving A_1–A_4, we take α_1, α_2, β_1, and β_2 as known variables, then, (17) can be regarded as an eighth-order nonhomogeneous linear system of equations for A_1, A_2, A_3, and A_4. According to the method of solving linear equations mathematically, if there is a unique solution for A_1, A_2, A_3, A_4, the rank of the coefficient matrix M and the augmented matrix M_{AU} should be four. Since M is an 8×4 matrix, its rank is determined to be four. M_{AU} is shown in (A1), and m_{xy} is the element of the xth row and yth column of the matrix M. For M_{AU}, in order to make the rank to be four, its fifth-order subforms should be zero. According to these requirements, (A2) can be obtained for α_1, α_2, β_1, and β_2 as in the following:

$$M_{\mathrm{AU}} = \begin{bmatrix} m_{11} & m_{12} & m_{13} & m_{14} & 0 \\ m_{21} & m_{22} & m_{23} & m_{24} & 0 \\ m_{31} & m_{32} & m_{33} & m_{34} & 0 \\ m_{41} & m_{42} & m_{43} & m_{44} & 0 \\ m_{51} & m_{52} & m_{53} & m_{54} & 0 \\ m_{61} & m_{62} & m_{63} & m_{64} & 0 \\ m_{71} & m_{72} & m_{73} & m_{74} & \frac{\left(\alpha_1^2+\beta_1^2\right)\left(\alpha_2^2+\beta_2^2\right)V_{\mathrm{in}}}{1-D} D \\ m_{81} & m_{82} & m_{83} & m_{84} & \frac{\left(\alpha_1^2+\beta_1^2\right)\left(\alpha_2^2+\beta_2^2\right)V_{\mathrm{in}}}{1-D} \end{bmatrix} \tag{A1}$$

$$\begin{cases} m_{34}P - m_{31}P_1 - m_{32}P_2 - m_{33}P_3 = 0 \\ m_{44}P - m_{41}P_1 - m_{42}P_2 - m_{43}P_3 = 0 \\ m_{64}P - m_{61}P_1 - m_{62}P_2 - m_{63}P_3 = 0 \\ \left(Dm_{84} - m_{74}\right)P - \left(Dm_{81} - m_{71}\right)P_1 \\ \quad - \left(Dm_{82} - m_{72}\right)P_2 - \left(Dm_{83} - m_{73}\right)P_3 = 0 \end{cases} \tag{A2}$$

TABLE III
Numerical Solutions of (A1)

D	α_1	α_2	β_1	β_2
0.1	-0.1567	-0.4714	5.7099	11.6284
0.2	-0.4654	-1.0670	5.3005	11.2506
0.3	-0.8081	-1.5590	5.0080	11.0654
0.4	-1.1621	-1.9890	4.7829	10.9510
0.5	-1.5321	-2.3940	4.5971	10.8680
0.6	-1.9340	-2.8042	4.4340	10.8002
0.7	-2.3971	-3.2542	4.2813	10.7382
0.8	-2.9860	-3.8067	4.1270	10.6739
0.9	-3.5078	-4.2734	3.9885	10.6113

where the matrices P, P_1, P_2, and P_3 are

$$P = \begin{bmatrix} m_{11} & m_{12} & m_{13} \\ m_{21} & m_{22} & m_{23} \\ m_{51} & m_{52} & m_{53} \end{bmatrix} \quad P_1 = \begin{bmatrix} m_{14} & m_{12} & m_{13} \\ m_{24} & m_{22} & m_{23} \\ m_{54} & m_{52} & m_{53} \end{bmatrix}$$

$$P_2 = \begin{bmatrix} m_{11} & m_{14} & m_{13} \\ m_{21} & m_{24} & m_{23} \\ m_{51} & m_{54} & m_{53} \end{bmatrix} \quad P_3 = \begin{bmatrix} m_{11} & m_{12} & m_{14} \\ m_{21} & m_{22} & m_{24} \\ m_{51} & m_{52} & m_{54} \end{bmatrix}.$$

By solving (A2), the values of α_1, α_2, β_1, and β_2 can be obtained. Then, (17) can be simplified as (A3); taking α_1, α_2, β_1, and β_2 into (A3), A_1–A_4 can be calculated easily

$$\begin{bmatrix} m_{31} & m_{32} & m_{33} & m_{34} \\ m_{41} & m_{42} & m_{43} & m_{44} \\ m_{61} & m_{62} & m_{63} & m_{64} \\ m_{81} & m_{82} & m_{83} & m_{84} \end{bmatrix} \begin{bmatrix} A_1 \\ A_2 \\ A_3 \\ A_4 \end{bmatrix} = \frac{\left(\alpha_1^2+\beta_1^2\right)\left(\alpha_2^2+\beta_2^2\right)V_{\mathrm{in}}}{1-D} \begin{bmatrix} 0 \\ 0 \\ 0 \\ 1 \end{bmatrix}. \tag{A3}$$

It can be seen from (A2) that the solutions of α_1, α_2, β_1, and β_2 are only related to the duty cycle D of the switch. Due to the complexity of (A2), its algebraic solution is difficult to find. Luckily, the numerical solution with higher precision can be easily obtained by MATLAB, and can meet the requirements of practical engineering. The numerical solutions of (A2) with different duty cycles are given in Table III.

Then, the unknowns A_1, A_2, A_3, and A_4 in (17) can be expressed as

$$\begin{bmatrix} A_1 \\ A_2 \\ A_3 \\ A_4 \end{bmatrix} = \frac{\left(\alpha_1^2+\beta_1^2\right)\left(\alpha_2^2+\beta_2^2\right)V_{\mathrm{in}}}{1-D} \times \begin{bmatrix} m_{31} & m_{32} & m_{33} & m_{34} \\ m_{41} & m_{42} & m_{43} & m_{44} \\ m_{61} & m_{62} & m_{63} & m_{64} \\ m_{81} & m_{82} & m_{83} & m_{84} \end{bmatrix}^{-1} \begin{bmatrix} 0 \\ 0 \\ 0 \\ 1 \end{bmatrix}. \tag{A4}$$

REFERENCES

[1] J. M. Alonso, G. Martínez, M. Perdigão, M. R. Cosetin, and R. N. do Prado, "A systematic approach to modeling complex magnetic devices using SPICE: Application to variable inductors," *IEEE Trans. Power Electron.*, vol. 31, no. 11, pp. 7735–7746, Nov. 2016.

[2] H. Zhang, S. C. Wong, C. K. Tse, and X. Ma, "Study of parasitic and stray components induced ringings in class E power amplifiers in MHz range," in *Proc. Eur. Conf. Circuit Theory Des.*, 2005, pp. 129–132.

[3] B. Sun, Z. Zhang, and M. A. E. Andersen, "A comparison review of the resonant gate driver in the silicon MOSFET and the GaN transistor application," *IEEE Trans. Ind. Appl.*, vol. 55, no. 6, pp. 7776–7786, Nov./Dec. 2019.

[4] B. Sun, Z. Zhang, and M. A. E. Andersen, "Research of low inductance loop design in GaN HEMT application," in *Proc. 44th Annu. Conf. IEEE Ind. Electron. Soc.*, Washington, DC, USA, 2018, pp. 1466–1470.

[5] N. Huang *et al.*, "Power quality disturbances classification using rotation forest and multi-resolution fast S-transform with data compression in time domain," *IET Gener. Transmiss. Distrib.*, vol. 13, no. 22, pp. 5091–5101, Nov. 2019.

[6] D. J. Perreault *et al.*, "Opportunities and challenges in very high frequency power conversion," in *Proc. 24th Annu. IEEE Appl. Power Electron. Conf. Expo.*, 2009, pp. 1–14.

[7] A. Knott *et al.*, "Evolution of very high frequency power supplies," *IEEE J. Emerg. Sel. Topics Power Electron.*, vol. 2, no. 3, pp. 386–394, Sep. 2014.

[8] M. Liu, M. Fu, and C. Ma, "Parameter design for a 6.78-MHz wireless power transfer system based on analytical derivation of class E current-driven rectifier," *IEEE Trans. Power Electron.*, vol. 31, no. 6, pp. 4280–4291, Jun. 2016.

[9] L. Olivia, "*Radio frequency dc–dc converters: Device characterization, topology evaluation, and design*," Ph.D. dissertation, Dept. Elect. Eng. Comput. Sci., Massachusetts Inst. Technol., Cambridge, MA, USA, 2008.

[10] R. C. N. Pilawa-Podgurski, "*Design and evaluation of a very high frequency dc/dc converter*," M.Eng. thesis, Dept. Elect. Eng. Comput. Sci., Massachusetts Inst. Technol., Cambridge, MA, USA, 2007.

[11] J. W. Phinney, "*Multi-resonant passive components for power conversion*," Ph.D. dissertation, Dept. Elect. Eng. Comput. Sci., Massachusetts Inst. Technol., Cambridge, MA, USA, Jun. 2005.

[12] J. Warren, III, "*Cell-modulated resonant dc/dc power converter*," Master's thesis, Dept. Elect. Eng. Comput. Sci., Massachusetts Inst. Technol., Cambridge, MA, USA, Aug. 2005.

[13] J. M. Rivas, D. Jackson, O. Leitermann, A. D. Sagneri, Y. Han, and D. J. Perreault, "Design considerations for very high frequency dc–dc converters," in *Proc. 37th IEEE Power Electron. Spec. Conf.*, Jeju, South Korea, 2006, pp. 1–11.

[14] Y. Guan *et al.*, "Analysis and design of high-frequency converter with resistive matching network and spiral inductor," *IEEE Trans. Power Electron.*, vol. 33, no. 6, pp. 5062–5075, Jun. 2018.

[15] A. J. Hanson, J. A. Belk, S. Lim, C. R. Sullivan, and D. J. Perreault, "Measurements and performance factor comparisons of magnetic materials at high frequency," *IEEE Trans. Power Electron.*, vol. 31, no. 11, pp. 7909–7925, Nov. 2016.

[16] J. Hu, A. D. Sagneri, J. M. Rivas, Y. Han, S. M. Davis, and D. J. Perreault, "High-frequency resonant SEPIC converter with wide input and output voltage ranges," *IEEE Trans. Power Electron.*, vol. 27, no. 1, pp. 189–200, Jan. 2012.

[17] Z. Zhang, J. Lin, Y. Zhou, and X. Ren, "Analysis and decoupling design of a 30 MHz resonant SEPIC converter," *IEEE Trans. Power Electron.*, vol. 31, no. 6, pp. 4536–4548, Jun. 2016.

[18] R. C. N. Pilawa-Podgurski, A. D. Sagneri, J. M. Rivas, D. I. Anderson, and D. J. Perreault, "Very high frequency resonant boost converters," in *Proc. IEEE Power Electron. Spec. Conf.*, Orlando, FL, USA, 2007, pp. 2718–2724.

[19] M. Madsen, A. Knott, and M. A. E. Andersen, "Low power very high frequency resonant converter with high step down ratio," in *Proc. Africon*, Pointe-Aux-Piments, Mauritius, 2013, pp. 1–6.

[20] L. Gu, Z. Tong, W. Liang, and J. Rivas-Davila, "A Multi-resonant gate driver for high-frequency resonant converters," *IEEE Trans. Ind. Electron.*, vol. 67, no. 2, pp. 1405–1414, Feb. 2020.

[21] Y. Guan, Y. Wang, W. Wang, and D. Xu, "A 20 MHz low-profile dc–dc converter with magnetic-free characteristics," *IEEE Trans. Ind. Electron.*, vol. 67, no. 2, pp. 1555–1567, Feb. 2020.

[22] W. Liang *et al.*, "Low mass RF power inverter for cubesat plasma thruster using 3D printed inductors," in *Proc. Workshop Control Model. Power Electron.*, 2016, pp. 1–7.

[23] S. Aldhaher, P. C. K. Luk, K. El Khamlichi Drissi, and J. F. Whidborne, "High-input-voltage high-frequency class E rectifiers for resonant inductive links," *IEEE Trans. Power Electron.*, vol. 30, no. 3, pp. 1328–1335, Mar. 2015.

[24] L. C. Raymond, W. Liang, and J. M. Rivas-Davila, "Performance evaluation of diodes in 27.12 MHz class-D resonant rectifiers under high voltage and high slew rate conditions," in *Proc. Workshop Control Model. Power Electron.*, 2014, pp. 1–9.

[25] L. Gu, K. Surakitbovorn, G. Zulauf, S. Chakraborty, and J. Rivas-Davila, "High-Frequency bidirectional resonant converter for high conversion ratio and variable load operation," in *Proc. IEEE 19th Workshop Control Model. Power Electron.*, Padua, Italy, 2018, pp. 1–8.

[26] W. Liang, J. Glaser, and J. Rivas, "13.56 MHz high density dc–dc converter with PCB inductors," in *Proc. 28th Annu. IEEE Appl. Power Electron. Conf. Expo.*, 2013, pp. 633–640.

[27] M. K. Kazimierczuk, "Analysis of class E zero-voltage-switching rectifier," *IEEE Trans. Circuits Syst.*, vol. 37, no. 6, pp. 747–755, Jun. 1990.

[28] Y. Guan, Y. Wang, W. Wang, and D. Xu, "A High-performance isolated high-frequency converter with optimal switch impedance," *IEEE Trans. Ind. Electron.*, vol. 66, no. 7, pp. 5165–5176, Jul. 2019.

[29] L. Raymond, W. Liang, J. Choi, and J. Rivas, "27.12 MHz large voltage gain resonant converter with low voltage stress," in *Proc. IEEE Energy Convers. Congr. Expo.*, 2013, pp. 1814–1821.

[30] H. Jedi, A. Reatti, and M. K. Kazimierczuk, "A current-source sinusoidal gate driver for high-frequency applications," in *Proc. IEEE Int. Symp. Circuits Syst.*, 2018, pp. 1–5.

Yueshi Guan (Member, IEEE) was born in Heilongjiang, China, in 1990. He received the B.S., M.S., and Ph.D. degrees in electrical engineering from the Harbin Institute of Technology (HIT), Harbin, China, in 2013, 2015, and 2019, respectively.

Since 2019, he has been an Associate Professor with the Department of Electrical and Electronics Engineering, HIT. His research interests are in the areas of high-frequency and very high-frequency converters, single-stage ac/dc converter, and light-emitting diode lighting systems.

Chang Liu (Student Member, IEEE) was born in Jilin, China, in 1997. She received the B.S. degree in electrical engineering in 2019 from the Harbin Institute of Technology, Harbin, China, where she is currently working toward the M.S. degree in electrical engineering.

Her current research interests include high-frequency and very-high -frequency converters.

Yijie Wang (Senior Member, IEEE) was born in Heilongjiang, China, in 1982. He received the B.S., M.S., and Ph.D. degrees in electrical engineering from the Harbin Institute of Technology, Harbin, China, in 2005, 2007, and 2012, respectively.

From 2012 to 2014, he was a Lecturer with the Department of Electrical and Electronics Engineering, Harbin Institute of Technology. Since 2015, he has been an Associate Professor with the Department of Electrical and Electronics Engineering, Harbin Institute of Technology. His research interests include dc–dc converters, soft-switching power converters, power factor correction circuits, digital control electronic ballasts, and light-emitting diode lighting systems.

Dr. Wang is an Associate Editor for the IEEE TRANSACTIONS ON INDUSTRIAL ELECTRONICS, *Institution of Engineering and Technology (IET) Power Electronics*, and *Journal of Power Electronics*.

Wei Wang was born in Heilongjiang, China, in 1963. She received the B.S. degree in automatic test and control, the M.S. degree in electrical engineering, and the Ph.D. degree in mechanical electronic engineering from the Harbin Institute of Technology, Harbin, China, in 1984, 1990, and 2002, respectively.

Since 2003, she has been a Professor with the Department of Electrical Engineering, Harbin Institute of Technology. Her research interests include soft-switching converters, digital control electronic ballast, and regenerative energy converter technique.

Dianguo Xu (Fellow, IEEE) was born in Heilongjiang, China, in 1960. He received the B.S. degree in control engineering from Harbin Engineering University, Harbin, China, in 1982, and the M.S. and Ph.D. degrees in electrical engineering from the Harbin Institute of Technology (HIT), Harbin, in 1984 and 1989, respectively.

In 1984, he joined the Department of Electrical Engineering, HIT, as an Assistant Professor. Since 1994, he has been a Professor with the Department of Electrical Engineering, HIT. From 2000 to 2010, he was the Dean of the School of Electrical Engineering and Automation, HIT. He is now the Vice President of HIT. He has authored or coauthored more than 600 technical papers. His research interests include renewable energy generation technology, power quality mitigation, sensorless vector controlled motor drives, high-performance servo system.

Dr. Xu is an Associate Editor for the IEEE TRANSACTIONS ON INDUSTRIAL ELECTRONICS, IEEE TRANSACTIONS ON POWER ELECTRONICS, and IEEE JOURNAL OF EMERGING AND SELECTED TOPICS IN POWER ELECTRONICS. He is the Chairman of the IEEE Harbin Section.